ELSEVIER

Contents lists available at ScienceDirect

# Ceramics International

journal homepage: www.elsevier.com/locate/ceramint





# Effects of Al substitution with Si and Sn on tribological performance of Ti<sub>3</sub>AlC<sub>2</sub>

Leping Cai <sup>a,b</sup>, Zhenying Huang <sup>a,\*</sup>, Wenqiang Hu <sup>a</sup>, Yexiao Chen <sup>b</sup>, Zeyi Tan <sup>b</sup>, Miladin Radovic <sup>b,\*\*</sup>

- a Centre of Materials Science and Engineering, School of Mechanical and Electronic Control Engineering, Beijing Jiaotong University, Beijing, 100044, China
- <sup>b</sup> Department of Materials Science & Engineering, Texas A&M University, College Station, TX, 77843, USA

#### ARTICLE INFO

Keywords: MAX phases A-site solid solutions Dry sliding behavior Self-generated film Tribo-oxidation

#### ABSTRACT

Since their discovery, the MAX phases have elicited engineering interest as potential choices for wear resistant parts. One such compound is  $Ti_3AlC_2$  with nano-layered structure, low density (4.25 g/cm³), good oxidation resistant and self-lubrication properties. The purpose of this investigation was to evaluate the dominant effect of the A-site solid solution elements addition on dry sliding characteristics of  $Ti_3AlC_2$  against 0.45% C steel (S45C) disk, a material which is widely used in wear-critical applications such as impeller, gear and axles. Dry sliding tribological behaviors of hot-pressed  $Ti_3Al_{0.94}C_2$ ,  $Ti_3Al_{0.78}Sn_{0.22}C_2$  and  $Ti_3Al_{0.67}Si_{0.28}C_2$  solid solutions were conducted using a block-on-disk type tester at surface sliding speed range from 10 to 30 m/s and in the normal load range from 20 to 80 N. The results show that friction coefficient of  $Ti_3Al_{0.94}C_2$  is higher than that of  $Ti_3Al_{0.78}Sn_{0.22}C_2$ , but lower than that of  $Ti_3Al_{0.67}Si_{0.28}C_2$ . However, the change in wear rate as a function of normal load for different sliding speed shows almost reversed trend. Difference in the phase composition of friction films were found to be responsible for observed change in tribological behaved after partial substitution of Al in  $Ti_3AlC_2$  with Sn and Si. This study shows that friction coefficient of  $Ti_3AlC_2$  can be adjusted from 0.2 to 0.38 by partially substituting Al with Si and/or Sn.

# 1. Introduction

Advanced materials with lower wear rate, appropriate and steady friction coefficient that can be applied over a wide range of conditions have been of the particular interests for different industrial applications in recent years [1–3]. Numerous studies have shown that  $M_{n+1}AX_n$  phases (where M is an early transition metal, A is mostly a group IIIA or IVA element, X is either C or N, and n = 1, 2 or 3) can show good tribological performance combined with excellent thermal shock resistance, thermal and electrical conductivity, and in some cases good oxidation resistance and crack healing ability [4–10]. It is attributed to the unique nano-layered, hexagonal crystallographic structure that ceramic (MX) layers are interleaved with weakly boned layers of A-site element of MAX phases.

The most studied MAX phase with promising applications as high temperature wear resistant material is  $Ti_3AlC_2$  because of low density  $(4.25~g/cm^3)$ , good oxidation resistant and self-lubrication properties

[4-6,9,11-17]. The formation of self-generating wear resistance tribo-film on the contact surface, that contains mostly Al oxide, is a crucial for understanding observed tribological behavior of Ti<sub>3</sub>AlC<sub>2</sub> [13, 18]. Formation of this tribo-film is attributed primarily to the decomposition of MAX phases by diffusion of weakly bonded Al towards contact surface under external effects such as mechanical loading and elevated temperatures, and its reaction with ambient air to form oxides during dry sliding processes. The similar phenomenon also leads to a good oxidation resistance and crack self-healing ability of Ti<sub>3</sub>AlC<sub>2</sub> [9, 19–22]. For example, small cracks in Ti<sub>3</sub>AlC<sub>2</sub> can completely self-heal as they became filled with predominately Al<sub>2</sub>O<sub>3</sub> at high temperature in air. This preferential oxidation to form predominately Al<sub>2</sub>O<sub>3</sub> is due to the high activity and diffusivity of Al in Ti<sub>3</sub>AlC<sub>2</sub> [19]. It has been also shown that when using Ti<sub>3</sub>AlC<sub>2</sub> as reinforced phases to prepare metal matrix composites, the easy diffusion of Al out of MAX phase to metallic phase such as Cu, Ni, NiTi or TiAl results in solid solution strengthening of metallic phase and/or formation of complex intermetallic compounds

E-mail addresses: zhyhuang@bjtu.edu.cn (Z. Huang), mradovic@tamu.edu (M. Radovic).

<sup>\*</sup> Corresponding author.

<sup>\*\*</sup> Corresponding author.

[23–26]. The latter can even result in the formation of composite with sub-stoichiometric  $TiC_x$  phases formed as a result decomposition of  $Ti_3AlC_2$ , and metal matrix with the improved mechanical properties [26].

Formation of the tribo-film on MAX phases depends on external friction conditions such as sliding speed and normal load [13,27-29]. The tribo-film on MAX phases was found to be thicker, smother and more continuous in case of high frictional speeds, especially on Ti<sub>3</sub>AlC<sub>2</sub> that is one of the candidates for high-speed tribological applications. However, the application of Ti<sub>3</sub>AlC<sub>2</sub> for structural components can be limited due to its relatively lower hardness and strength, and thus solid solution strengthening and hardening effects have been explored for Ti<sub>3</sub>AlC<sub>2</sub> and other MAX phases [30-38]. Partially substitution of Al in Ti<sub>3</sub>AlC<sub>2</sub> by Si or Sn to form Ti<sub>3</sub>Al(Si)C<sub>2</sub> and Ti<sub>3</sub>Al(Sn)C<sub>2</sub> solid solutions was widely studied [30-37]. For example, Zhou et al. [32] revealed that Vickers hardness, flexural strength and compressive strength of Ti<sub>3</sub>Al<sub>0.75</sub>Si<sub>0.25</sub>C<sub>2</sub> solid solution was enhanced by 26%, 12% and 29%, respectively, when compared with pure Ti<sub>3</sub>AlC<sub>2</sub>. Gao et al. [34] synthesized a serious of Ti<sub>3</sub>(A<sub>l-x</sub>Si<sub>x</sub>)C<sub>2</sub>, they reported that Vickers hardness of  $Ti_3Al_{0.4}Si_{0.6}C_2$  was 5.6  $\pm$  0.2 GPa, much higher than that of  $Ti_3AlC_2$ (4.1  $\pm$  0.14 GPa) and Ti<sub>3</sub>SiC<sub>2</sub> (4.2  $\pm$  0.37 GPa), and the elastic moduli increased monotonically as increasing from 0 to 1. Huang and Xu et al. [35,36] synthesized Ti<sub>3</sub>AlSn<sub>0.2</sub>C<sub>2</sub> and Ti<sub>3</sub>Al<sub>0.8</sub>Sn<sub>0.4</sub>C<sub>2</sub> solid solutions by hot-pressed sintering method and reported that flexural strengths of the two compounds to be 560 MPa and 620 MPa, respectively, i.e. almost 51% and 67% higher than that of pure Ti<sub>3</sub>AlC<sub>2</sub> (~370 MPa). Interestingly, Huang et al. [36] further reported that the friction coefficient of Ti<sub>3</sub>AlC<sub>2</sub> increases from 0.13 to 0.16 to 0.26-0.30 and 0.30-0.33 when dry sliding against low-carbon steel under the normal load range of 20-80 N after the substitution of 20% and 40% of Al with Sn, respectively, at a sliding speed of 30 m/s. Thus, they revealed that Ti<sub>3</sub>Al<sub>x</sub>Sn<sub>1-x</sub>C<sub>2</sub> could be adjusted to fall within the friction coefficient range of 0.13-0.33 after adding different amounts of Sn and tailor it for wide range of tribological conditions. With exception of that study, all other studies on Ti<sub>3</sub>Al<sub>x</sub>Sn<sub>1-x</sub>C<sub>2</sub> and Ti<sub>3</sub>Al<sub>x</sub>Si<sub>1-x</sub>C<sub>2</sub> solid solutions have mainly been focused on synthesis, structural and mechanical performance, while the tribological mechanism has not received much attention.

This study reports on the dry sliding behaviors of  $Ti_3AlC_2$ ,  $Ti_3Al_{0.8}Sn_{0.2}C_2$  and  $Ti_3Al_{0.8}Si_{0.2}C_2$  against 0.45% C steel (S45C) at the same conditions within a sliding speed of 10–30 m/s under normal loads from 20 to 80 N. Tribological performance of these three samples were MAX phase compositions in terms of friction coefficient, wear rates, microstructures of friction surface and phase composition of tribo-film. The microstructure and phase composition of friction surfaces were characterized using scanning electron microscopy, energy dispersive X-ray spectroscopy, electron probe microanalysis and X-ray photoelectron spectroscopy techniques. The effects of partial substitution of Al with different A-site elements on tribological properties of  $Ti_3AlC_2$  were also discussed.

## 2. Experimental procedures

## 2.1. Materials preparation

Ti<sub>3</sub>AlC<sub>2</sub>, Ti<sub>3</sub>Al<sub>0.8</sub>Sn<sub>0.2</sub>C<sub>2</sub> and Ti<sub>3</sub>Al<sub>0.8</sub>Si<sub>0.2</sub>C<sub>2</sub> aggregates were synthesized from reactant (starting) powder mixtures consisting of Ti (48 μm average particle size, 99.5 wt% purity), Al (75 μm average particle size, 99.5 wt% purity), Si (75 μm average particle size, 99.5 wt% purity), Si (75 μm average particle size, 99.5 wt% purity) and TiC (48 μm average particle size, 99.5 wt% purity) all from Sinopharm Chemical Reagent Co., Ltd. (China). Powders were weighed to achieve molar ratios of Ti: Al:C = 1:1.1:1.85, Ti:Al:Si:C = 1:1:0.2:1.85 and Ti:Al:Sn:C = 1:1:0.2:1.85. Excess Al was added to the starting powder mixtures to compensate the loss due to Al volatilization during the reaction sintering process, and deficient amount of C was also introduced into the starting

composition to obtain a single phase, as recommended in other reports [36,37]. The as-synthesized Ti<sub>3</sub>AlC<sub>2</sub>, Ti<sub>3</sub>Al<sub>0.8</sub>Sn<sub>0.2</sub>C<sub>2</sub> and Ti<sub>3</sub>Al<sub>0.8</sub>Si<sub>0.2</sub>C<sub>2</sub> aggregates were ground into powder (~200 mesh) by high energy ball milling. Those powders were further reaction sintered in fully dense samples following procedure reported elsewhere [33]. To make friction specimens, sintered material was cut into 10 mm  $\times$  10 mm  $\times$  12 mm samples by electro-discharge machining (EDM). The 10 mm  $\times$  10 mm sliding surfaces were polished using SiC-grit paper up to #800, ultrasonically cleaned in alcohol and finally dried.

Dry sliding tribological behaviors of the bulk samples were performed on a block-on-disk type tester that was described in more details elsewhere [39]. A S45C steel disk which is widely used in wear-critical applications such as impeller, gear and axles with hardness of 3.2  $\pm$  0.1 GPa and size of  $\Phi$ 300 mm imes 10 mm was selected as the friction counterpart. The steel counterpart is fixed above the sample stage so that the sample was always in contact with an area of 10 mm  $\times$  10 mm. The loading system of the tester is connecting and maintains balance with the sample stage through the oil hydraulic transmission system. When during the sliding process, the loading caused adequate oil pressure drives the sample stage to move up making the friction surface extrude with the counterpart, so that the frictional surface is always in extrusion contact with the counterpart even though the frictional surface is constantly being consumed during the sliding process. Friction tests were carried out with surface sliding speeds ranging from 10 to 30 m/s, and the normal load was applied in the range of 20-80 N for each sliding speed. A continuous sliding distance was kept as 12,000 m. The friction coefficient at any time was recorded automatically by data acquisition software connected to friction teste machine, and the wear rate was calculated as the following formula:

$$WR = \frac{\Delta m}{\rho FL}$$

Where WR refers to the wear rate, the unit is mm³/Nm;  $\Delta m$  is the mass loss before and after each friction test, the unit is g;  $\rho$  is the Volume density, which were calculated to be 4.19 g/cm³ for Ti<sub>3</sub>AlC<sub>2</sub>, 4.9 g/cm³ for Ti<sub>3</sub>Al<sub>0.8</sub>Sn<sub>0.2</sub>C<sub>2</sub> and 4.32 g/cm³ for Ti<sub>3</sub>Al<sub>0.8</sub>Si<sub>0.2</sub>C<sub>2</sub> [33,36]; F refers to the normal load, the unit is N; and L refers to the sliding distance, the unit is m.

The pre-abrasion was performed firstly when tested on each new sample or changed any of the sliding condition to eliminate any possible influence. The same sample should be tested three times under each condition to get the average value.

## 2.2. Phase and microstructure characterizations

Phase identification of the synthesized materials was identified by X-Ray Diffraction (XRD) analysis with Cu K $\alpha$  radiation (X' PERT-PRO MPDT, Netherlands). Microstructure and compositions of the friction surface and cross-section areas were analyzed using scanning electron microscope (SEM, ZEISS EVO 18, Germany) equipped with an energy dispersive X-ray spectrometer (EDS, Bruker Nano XFlash detector 5010) and an electron probe microanalysis (EPMA, Cameca SXFive, France) equipped with a wave dispersive spectroscopy (WDS). For each phase, the composition was determined in five point using WDS and their mean value calculated and reported herein. The chemical states of elements detected on the friction surface were further examined by X-ray Photoelectron Spectroscopy (XPS, ESCALAB 250Xi).

## 3. Results

## 3.1. Phase compositions of Ti<sub>3</sub>AlC<sub>2</sub>, Ti<sub>3</sub>Al<sub>0.8</sub>Sn<sub>0.2</sub>C<sub>2</sub>, Ti<sub>3</sub>Al<sub>0.8</sub>Si<sub>0.2</sub>C<sub>2</sub>

XRD diffraction spectra in Fig. 1a indicate that sintered  $Ti_3AlC_2$ ,  $Ti_3Al_{0.8}Si_{0.2}C_2$  and  $Ti_3Al_{0.8}Sn_{0.2}C_2$  samples were XRD pure, without any detectable XRD peaks that can be related to the common impurity

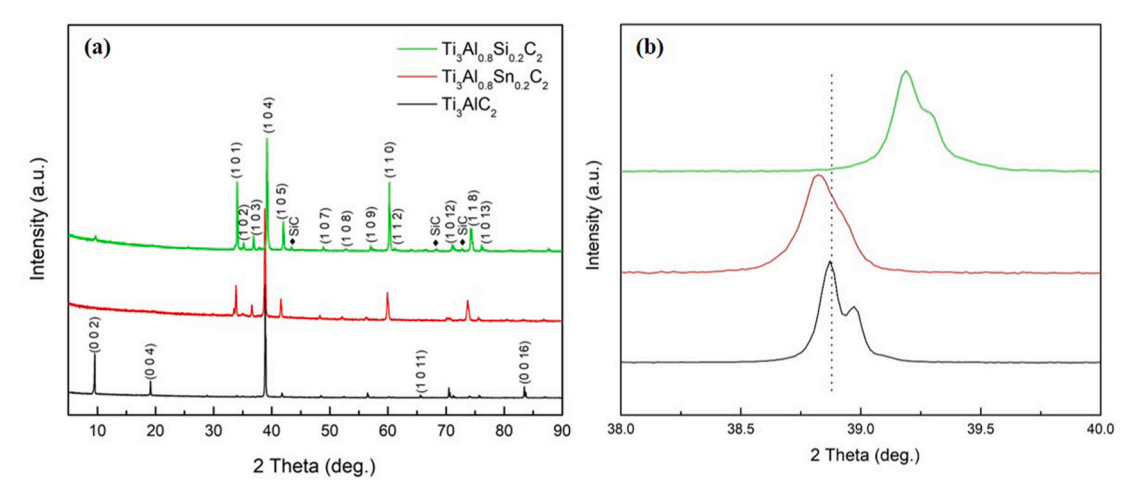


Fig. 1. (a) XRD patterns of bulk Ti<sub>3</sub>AlC<sub>2</sub>, Ti<sub>3</sub>Al<sub>0.8</sub>Sn<sub>0.2</sub>C<sub>2</sub> and Ti<sub>3</sub>Al<sub>0.8</sub>Si<sub>0.2</sub>C<sub>2</sub> with indexed peaks of MAX phase; (b) enlarged XRD patterns of (a).

phases such as TiC, Al<sub>3</sub>Ti, Ti<sub>6</sub>Sn<sub>5</sub> or Ti<sub>5</sub>Si<sub>3</sub>. Only minor peaks related to SiC secondary phases were detected in Ti<sub>3</sub>Al<sub>0.8</sub>Si<sub>0.2</sub>C<sub>2</sub>. As shown in the enlarged XRD pattern for selected peaks in Fig. 1b, the characteristic peaks shift with addition of the Si and Sn due to the lattice deformation caused by substitutions on the A-site. In addition, the average phase compositions of the sintered samples identified by EDS are also presented in Table 1 for all three samples. As it can be seen in Table 1, the composition of the sintered samples slightly deviates from the nominal (targeted) one due to volatilization of the low melting points A-site elements (especially Sn and Al) during reaction sintering, and thus final sintered samples had compositions Ti<sub>3</sub>Al<sub>0.94</sub>C<sub>2</sub>, Ti<sub>3</sub>Al<sub>0.78</sub>Sn<sub>0.22</sub>C<sub>2</sub> and Ti<sub>3</sub>Al<sub>0.67</sub>Si<sub>0.28</sub>C<sub>2</sub>. Note that the amount of carbon cannot be detected accurately in EDS, and thus it is assumed that Ti:C atomic ratio is 3:2 in all samples. Density, Vickers hardness and flexural strength reported in the previous studies [33,36] from the same set of samples, were also listed in Table 1 for comparison, and they suggest that solid solutions hardening and strengthening can be achieved in this system.

# 3.2. Friction coefficients and wear rates

Fig. 2a-c shows the variation curves of friction coefficient with normal load at different sliding speeds, for all three samples examined in this study. When at the low sliding speed of 10 m/s, friction coefficient of Ti<sub>3</sub>Al<sub>0.94</sub>C<sub>2</sub> increases from 0.25 to 0.33 accompanied by normal load increasing from 20 to 40 N, after that load it remains almost constant. However, for Ti<sub>3</sub>Al<sub>0.78</sub>Sn<sub>0.22</sub>C<sub>2</sub>, the friction coefficient is 0.35 under 20 N and it remains almost constant up to the normal load of 80 N, after some small fluctuations. For Ti<sub>3</sub>Al<sub>0.67</sub>Si<sub>0.28</sub>C<sub>2</sub>, when the normal load is 20 N, the corresponding friction coefficient is 0.32 and it increases to 0.38 under 30 N, after that remains almost constant with increasing normal loads to 80 N. At the medium sliding speed of 20 m/s (Fig. 2b), the friction coefficient only slightly increases from 0.24 to 0.25 for  $Ti_3Al_{0.94}C_2$ , from 0.23 to 0.29 for  $Ti_3Al_{0.78}Sn_{0.22}C_2$  and from 0.31 to 0.32 for  $Ti_3Al_{0.67}Si_{0.28}C_2$ , with normal load goes from 20 N to 80 N. when at higher sliding speed of 30 m/s, friction coefficients for Ti<sub>3</sub>Al<sub>0.94</sub>C<sub>2</sub>,  $Ti_3Al_{0.78}Sn_{0.22}C_2$  and  $Ti_3Al_{0.67}Si_{0.28}C_2$  are around 0.22, 0.2 and 0.25,

respectively, and remain almost constant as the normal load increases. Comparison of Fig. 2a–b clearly shows that friction coefficient notably reduces with increasing sliding speed from 10 to 30 m/s for all three samples, while it only slightly changes with increasing normal load, primarily at the lower sliding speeds and below critical normal loads of 20–40 N. Overall, the friction coefficient of  ${\rm Ti}_3{\rm Al}_{0.67}{\rm Si}_{0.28}{\rm C}_2$  is higher than that of  ${\rm Ti}_3{\rm Al}_{0.94}{\rm C}_2$ , and that of  ${\rm Ti}_3{\rm Al}_{0.78}{\rm Sn}_{0.22}{\rm C}_2$  for each sliding speed. This suggests that the friction coefficient of  ${\rm Ti}_3{\rm Al}_{0.94}{\rm C}_2$  could be adjusted by forming a  ${\rm Ti}_3{\rm Al}_{0.78}{\rm Sn}_{0.22}{\rm C}_2$  or  ${\rm Ti}_3{\rm Al}_{0.67}{\rm Si}_{0.28}{\rm C}_2$  solid solution to widen its application range.

Selected, but typical plots of friction coefficients vs. sliding distance collected under 80 N at sliding speeds of 10, 20 and 30 m/s in turn are shown in Fig. 2d–f, respectively. The initial transition behavior, during which the friction coefficient is slightly affected by sliding distance, can be observed in Fig. 2d–f, and it is most likely caused by the thermal instabilities of friction surfaces. After this transition, it reaches to the steady state in which coefficient of friction is almost impervious to sliding distance. However, friction coefficients show varying degrees of fluctuation in the steady state, which is most likely due to the interference of asperities between contact friction surface. The transition region before relatively steady state regime and the random fluctuation behavior are typical of the dry-sliding friction, and have been reported elsewhere [13,27,28,40].

Fig. 2g–i shows the variation curves of wear rate with normal load for different sliding speeds. The wear rate of  $Ti_3Al_{0.94}C_2$  increases slightly from  $2.04\times10^{-6}$  to  $2.43\times10^{-6}$  mm³/Nm when the normal load increases from 20 N to 80 N at 10 m/s. It also increases from  $2.52\times10^{-6}$  to  $3.2\times10^{-6}$  mm³/Nm along with normal load for  $Ti_3Al_{0.78}Sn_{0.22}C_2$ , while in the case of  $Ti_3Al_{0.67}Si_{0.28}C_2$ , it only varies slightly from  $3.47\times10^{-6}$  to  $3.42\times10^{-6}$  mm³/Nm. Nevertheless, the wear rate decreases from  $2.72\times10^{-6}$  to  $2.39\times10^{-6}$  mm³/Nm, and from  $4.67\times10^{-6}$  to  $3.2\times10^{-6}$  mm³/Nm with increasing normal load for  $Ti_3Al_{0.94}C_2$  and  $Ti_3Al_{0.78}Sn_{0.22}C_2$  at 20 m/s, respectively, while it slightly varies from  $2.51\times10^{-6}$  to  $2.68\times10^{-6}$  mm³/Nm for  $Ti_3Al_{0.67}Si_{0.28}C_2$ . As of 30 m/s for  $Ti_3Al_{0.94}C_2$ , the wear rate decreases slightly from  $3.12\times10^{-6}$  to  $2.9\times10^{-6}$  mm³/Nm, while it varies from  $4.2\times10^{-6}$  to  $4.68\times10^{-6}$  mm³/Nm, while it varies from  $4.2\times10^{-6}$  to  $4.68\times10^{-6}$  mm³/Nm,

Table 1 Elements compositions from EDS and stoichiometry formula of  $Ti_3AlC_2$ ,  $Ti_3Al_{0.8}Si_{0.2}C_2$  and  $Ti_3Al_{0.8}Sn_{0.2}C_2$  in this work, and density, Vickers hardness and flexural strength values referred from Ref. [33,36].

Nominal molecular formula	Composition (at.%) from EDS					Stoichiometry	Volume Density (g/	Vickers hardness	Flexural strength	
	Ti	Al	Sn	Si	С	formula	cm <sup>3</sup> )	(GPa)	(MPa)	
Ti <sub>3</sub> AlC <sub>2</sub>	52.79	16.58			30.63	Ti <sub>3</sub> Al <sub>0.94</sub> C <sub>2</sub>	4.19	3.1	375 [36]	
$Ti_3Al_{0.8}Sn_{0.2}C_2$	50.64	13.37	3.74		32.25	$Ti_3Al_{0.78}Sn_{0.22}C_2$	4.9	3.53	560 [36]	
$Ti_3Al_{0.8}Si_{0.2}C_2$	51.82	11.89		5.18	31.11	$Ti_{3}Al_{0.67}Si_{0.28}C_{2} \\$	4.32	5.3	609 [33]	

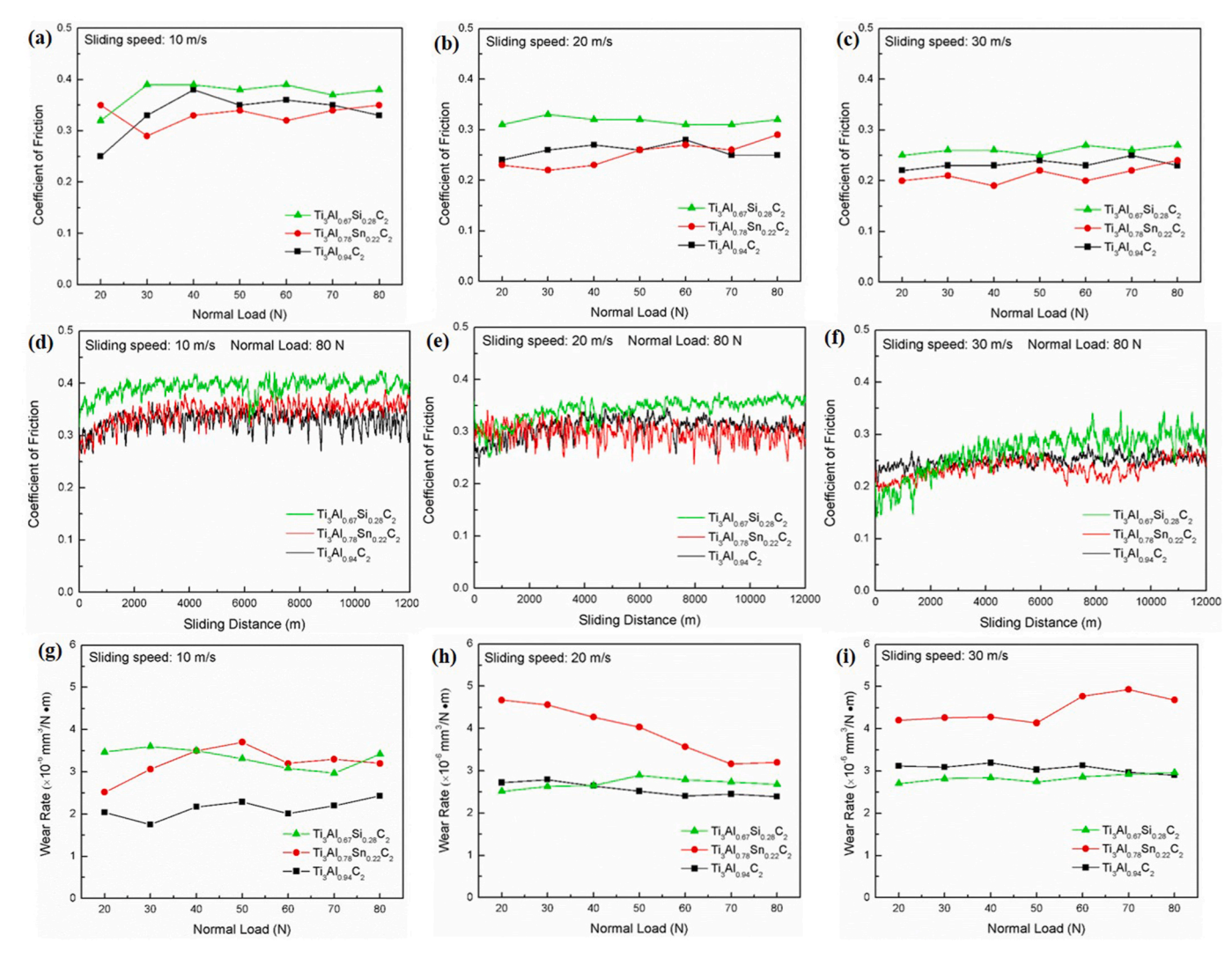


Fig. 2. (a), (b) and (c) show friction coefficients of  $Ti_3Al_{0.94}C_2$ ,  $Ti_3Al_{0.78}Sn_{0.22}C_2$  and  $Ti_3Al_{0.67}Si_{0.28}C_2$  as function of normal load for sliding speed of 10 m/s, 20 m/s and 30 m/s, respectively; (d), (e) and (f) show friction coefficients vs. sliding distance obtained under normal load of 80 N at sliding speed of 10 m/s, 20 m/s and 30 m/s, respectively; and (g), (h) and (i) show wear rates of  $Ti_3Al_{0.94}C_2$ ,  $Ti_3Al_{0.78}Sn_{0.22}C_2$  and  $Ti_3Al_{0.67}Si_{0.28}C_2$  as function of normal load at sliding speed of 10 m/s, 20 m/s and 30 m/s, respectively.

Nm for  $Ti_3Al_{0.78}Sn_{0.22}C_2$  and from  $2.7 \times 10^{-6}$  to  $2.96 \times 10^{-6}$  mm<sup>3</sup>/Nm for  $Ti_3Al_{0.67}Si_{0.28}C_2$ . In contrast to the observed difference of the friction coefficient with sliding rate discussed above, the speed-dependent performance of the wear rate in Fig. 2g–i suggest that the wear rate increases along with the sliding speed. In addition,  $Ti_3Al_{0.67}Si_{0.28}C_2$  with the larger friction coefficient but shows lower wear rate, especially at 30 m/s.

# 3.3. Friction surface characterization

Selected, but typical SEM images of the sliding surfaces of  $\rm Ti_3Al_{0.94}C_2$ ,  $\rm Ti_3Al_{0.78}Sn_{0.22}C_2$  and  $\rm Ti_3Al_{0.67}Si_{0.28}C_2$  after three successive tests for different sliding speed in each test, are shown in Fig. 3 to illustrate different features observed on the sliding surfaces. In addition, results of the quantitative EDS analysis in specific locations marked as A-L in Fig. 3, are provided in Table 2.

As it can be seen in Fig. 3 and Table 2, the fraction of sliding surface covered by tribo-oxide film for all three samples depends on the sliding speed. While the tribo-oxide film on the sliding surface is distributed discretely after the tests at  $10 \, \text{m/s}$ , the friction surface is almost covered by continuous tribo-film after testing at  $30 \, \text{m/s}$ . Evidence of tribo-film peeling, most likely due to the weak adhesion, shear stress and

fatigue, can be observed and higher sliding speeds, together with longitudinal crack and furrows on the friction surface. Part of wear debris was gradually crushed into the worn surface to generate continuous and impacted tribo-films as the sliding speed increases. The formation of tribo-films has been proven to prevent the worn surface from further deterioration, and consequently contributes to the low friction coefficient [13,27,28]. Previous study [39] also showed that surface roughness of self-generated film decrease with increasing the sliding speed by Atomic Force Microscopy (AFM). Therefore, it was reasonable to conclude that the smoother friction surfaces after testing at higher sliding speeds led to lower friction coefficients.

Table 2 lists the chemical composition of the sliding surface in different locations denoted in Fig. 3. It can be observed that the entire worn surface contained large amount of oxygen, suggesting that the tribo-film forms through tribo-oxidation reaction during the sliding process. Oxygen content in the regions with sporadic distribution of the film, such as in locations A, F, and I in Fig. 3, is lower than that in other regions covered by oxygen-rich tribo-films. It suggests that sufficient continuous tribo-films gradually grow on the friction surface. Small amount of iron is also detected in tribo-oxide film on the sliding surfaces by EDS, and it is most likely transferred from steel counterpart disk due to adhesive wear between the surfaces of tribological pairs.

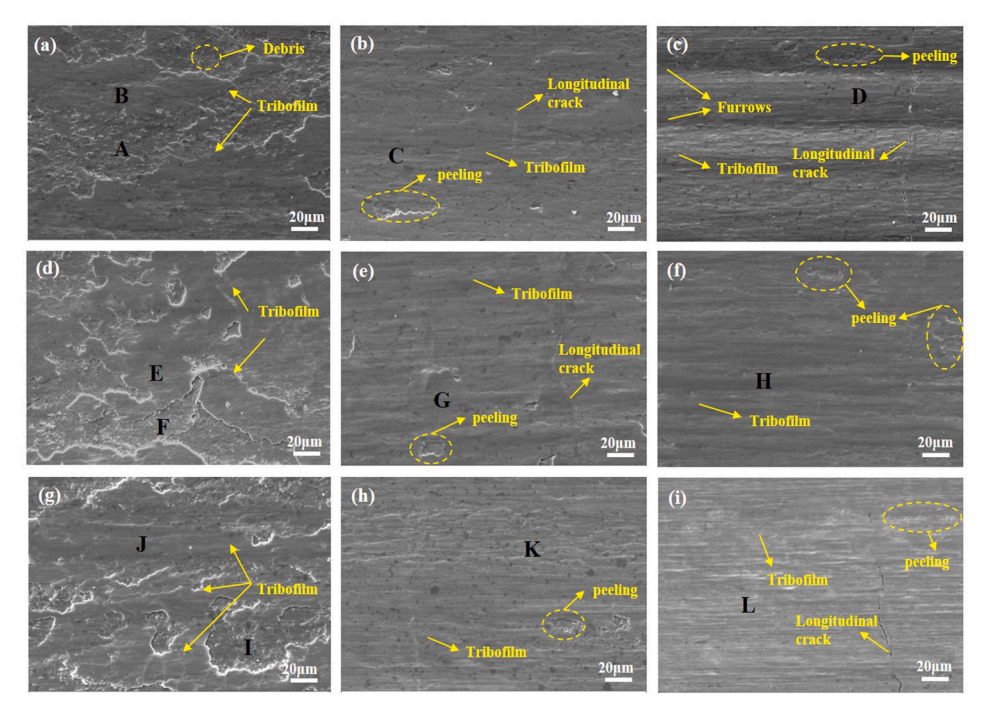


Fig. 3. SEM micrographs of sliding surfaces for  $Ti_3Al_{0.94}C_2$  after sliding speed at (a) 10 m/s, (b) 20 m/s and (c) 30 m/s; for  $Ti_3Al_{0.78}Sn_{0.22}C_2$  after sliding speed at (d) 10 m/s, (e) 20 m/s and (f) 30 m/s; and for  $Ti_3Al_{0.67}Si_{0.28}C_2$  after sliding speed at (g) 10 m/s, (h) 20 m/s and (i) 30 m/s under normal load of 80 N.

**Table 2**Results of the quantitative EDS analysis in specific locations denoted as A-L in Fig. 3.

Samples	Location	Ti at.%	Al at.%	Si at.%	Sn at.%	C at.%	O at.%	Fe at.%
В	18.6	5.0			7.4	57.7	11.4	
C	21.1	6.1			7.8	56.5	8.4	
D	16.3	4.8			8.2	58.5	12.2	
Ti <sub>3</sub> Al <sub>0.78</sub> Sn <sub>0.22</sub> C <sub>2</sub>	E	19.3	4.7		1.5	8.5	57.2	8.9
	F	32.3	8.8		2.3	27.3	27.4	1.9
	G	24.1	6.7		1.4	8.0	56.9	2.9
	Н	25.5	6.3		1.2	6.4	58.4	2.2
Ti <sub>3</sub> Al <sub>0.67</sub> Si <sub>0.28</sub> C <sub>2</sub>	I	34.5	10.6	3.3		29.8	10.9	1.0
	J	12.3	3.1	1.0		8	56.4	19.3
	K	27.8	7.5	2.7		15.4	43.7	3.0
	L	18.8	4.7	1.5		5.8	58.8	10.4

Additionally, even in the case of the formation of continuous tribo-oxide film at sliding rate of 30 m/s, its composition is not uniform, with regions richer in Ti and Al oxides and regions richer in Fe, as it is illustrated in Fig. 4 for  $\rm Ti_3Al_{0.94}C_2$  (results for  $\rm Ti_3Al_{0.78}Sn_{0.22}C_2$  and  $\rm Ti_3Al_{0.67}Si_{0.28}C_2$  were not show here but have an analogous appearance). Nevertheless, when those results are put in conjunction with the results of friction coefficient measurements in Fig. 2a–c, it is reasonable to conclude that the coverage of tribo-oxide film has a positive effect on friction performance.

Cross-sectional SEM micrographs through the friction surfaces for  $\rm Ti_3Al_{0.94}C_2,~Ti_3Al_{0.78}Sn_{0.22}C_2$  and  $\rm Ti_3Al_{0.67}Si_{0.28}C_2,$  after three successive tests under the normal load of 80 N, sliding speeds of 10--30~m/s and the sliding distance of 12,000~m in each test, together with corresponding WDS elemental maps and line analysis through the tribo-film are shown in Figs. 5–7, respectively. In all three figures, self-generated and continuous friction films can be observed attached to the friction surface. Thickness of the tribo-oxide film on  $\rm Ti_3Al_{0.94}C_2$  is  $0.85\text{--}0.93~\mu\text{m}$ , thus slightly larger than the thickness of tribo-oxide film of  $0.54\text{--}0.68~\mu\text{m}$  on  $\rm Ti_3Al_{0.78}Sn_{0.22}C_2$ , but lower than the thickness of the tribo-film of  $0.9\text{--}1.1~\mu\text{m}$  on  $\rm Ti_3Al_{0.67}Si_{0.28}C_2$ . Corresponding elemental WDS maps in Figs. 5–7 clearly show that the tribo-films consist of Ti, Al and Fe oxides

for Ti<sub>3</sub>Al<sub>0.94</sub>C<sub>2</sub>, Ti, Al, Fe and Sn oxides for Ti<sub>3</sub>Al<sub>0.78</sub>Sn<sub>0.22</sub>C<sub>2</sub>, and Ti, Al, Fe and Si for Ti<sub>3</sub>Al<sub>0.67</sub>Si<sub>0.28</sub>C<sub>2</sub>, which are in good agreement with EDS results summarized in Fig. 3 and Table 2. The tribo-film can be divided into different sub-scales, namely the outer, middle and inner one. For Ti<sub>3</sub>Al<sub>0.94</sub>C<sub>2</sub>, a thin Al-rich inner sub-scale can be observed, followed with Ti-rich middle sub-scale and relatively thick Fe and Ti rich outer subscale, Fig. 5b. For Ti<sub>3</sub>Al<sub>0.78</sub>Sn<sub>0.22</sub>C<sub>2</sub>, faint inner sub-scale rich in Ti and Sn, followed by a middle sub-scale consisting of primarily Ti and Al oxides, and thicker Fe oxides rich outer subscale can be observed in Fig. 6b. As of Ti<sub>3</sub>Al<sub>0.67</sub>Si<sub>0.28</sub>C<sub>2</sub>, inner and middle sub-scale consists primarily of Al, Si and Ti oxides, while outer sub-scale contains larger amount of Fe, Fig. 7b. Elemental WDS analysis through the tribo-oxide film in Figs. 5c, 6c and 7c also confirmed high Fe content close to the outer surface of the tribo-oxide film in all three MAX phases. Those results also show that contents of Al, Sn and Si increase moving from the outer towards inner sub-scale, and further to the substrate.

To further confirm that Ti, Al, Fe, Sn and Si detected in the tribo-film by EDS and WDS indeed form oxides, XPS analysis is employed in this study. Note here, that oxide phases in the tribo-film could not be identified with the high level of confidence using XRD of the sliding surface because of the very thin oxide scale with complex, multicomponent and

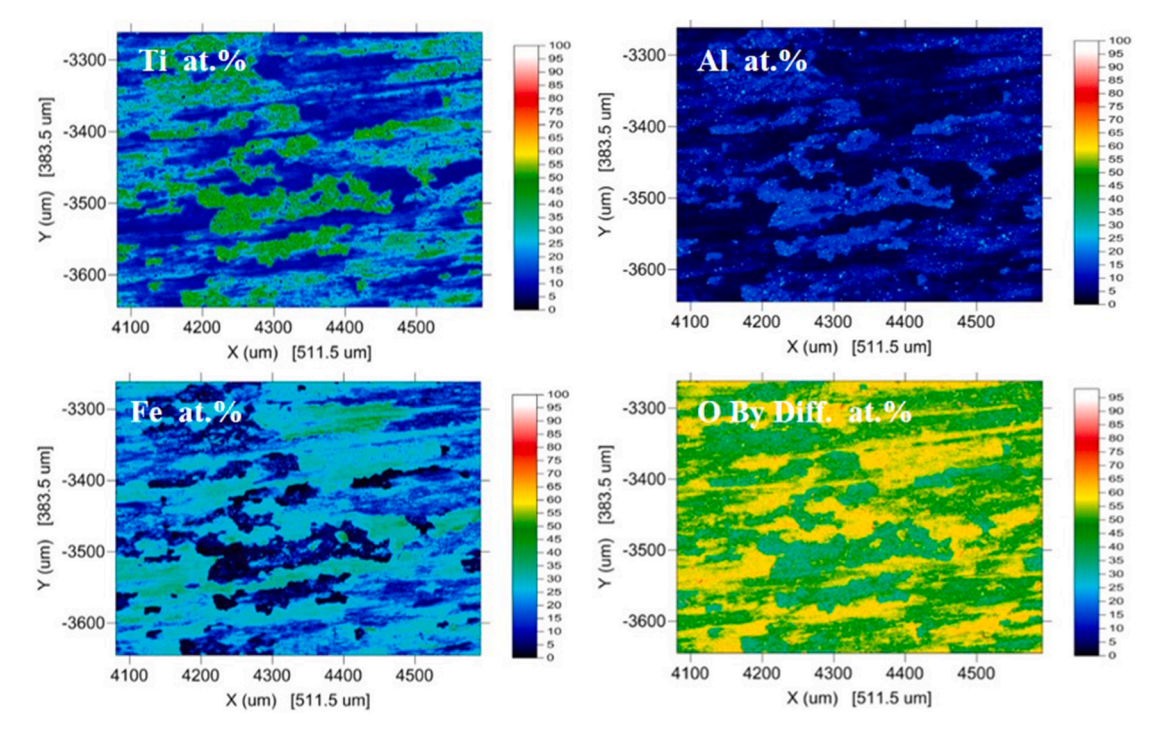


Fig. 4. Ti, Al, Fe and O EDS elemental maps of Ti<sub>3</sub>Al<sub>0.94</sub>C<sub>2</sub> sliding surface after testing at sliding speed of 30 m/s and normal load of 80 N.

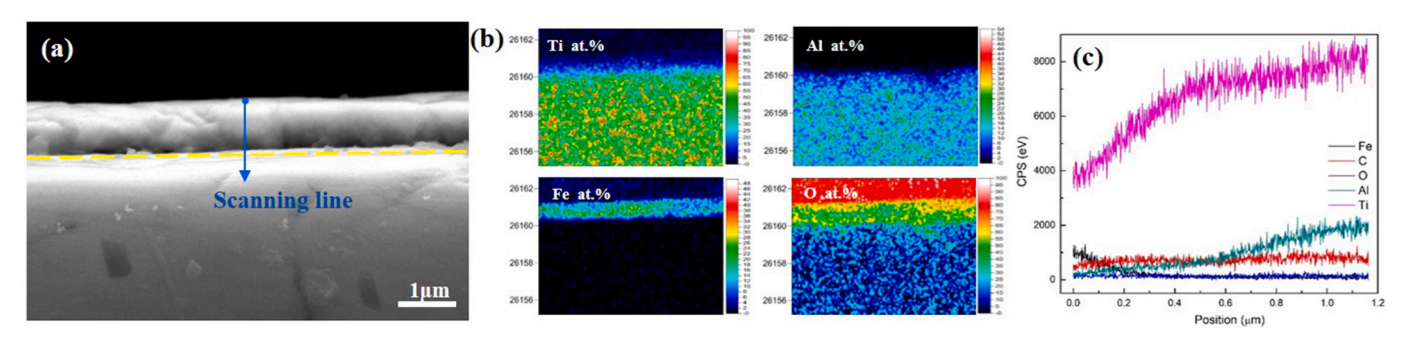


Fig. 5. (a) Cross-sectional SEM image, with (b) elemental WDS map and (c) elemental line analysis along the blue line of the frictional film for  $Ti_3Al_{0.94}C_2$  tested at sliding speed of 30 m/s and normal load of 80 N. The arrow line in (a) indicates the scanning direction from outer to inner position. (For interpretation of the references to colour in this figure legend, the reader is referred to the Web version of this article.)

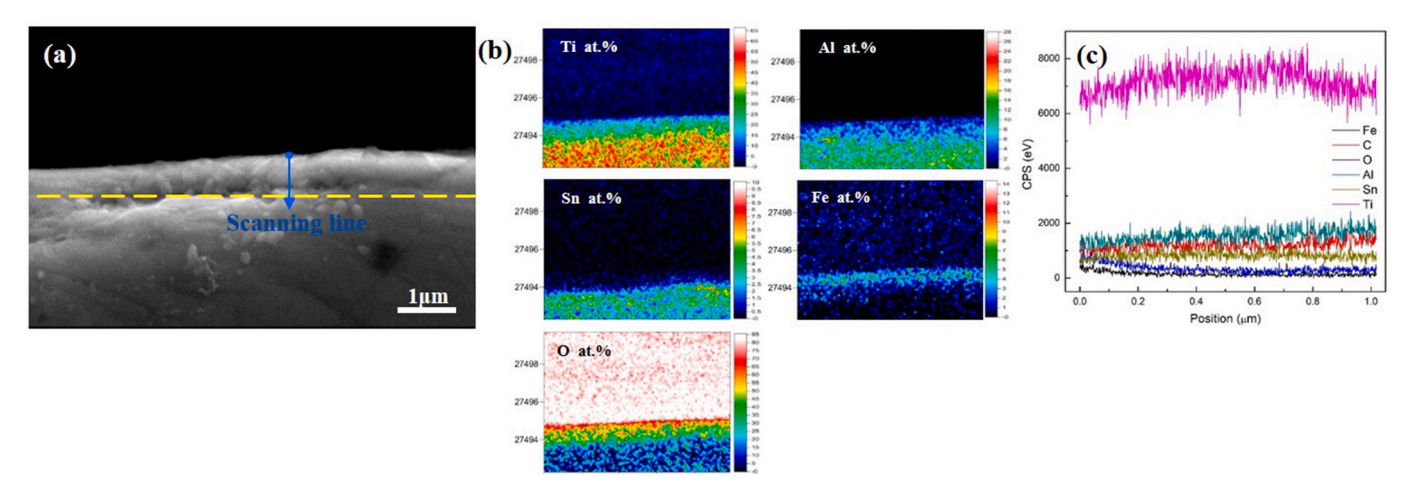


Fig. 6. (a) Cross-sectional SEM image, with (b) elemental WDS map and (c) elemental line analysis along the blue line of the frictional film (a) for  $Ti_3Al_{0.78}Sn_{0.22}C_2$  tested at sliding speed of 30 m/s and normal load of 80 N. The arrow line in (a) indicates the scanning direction from outer to inner position. (For interpretation of the references to colour in this figure legend, the reader is referred to the Web version of this article.)

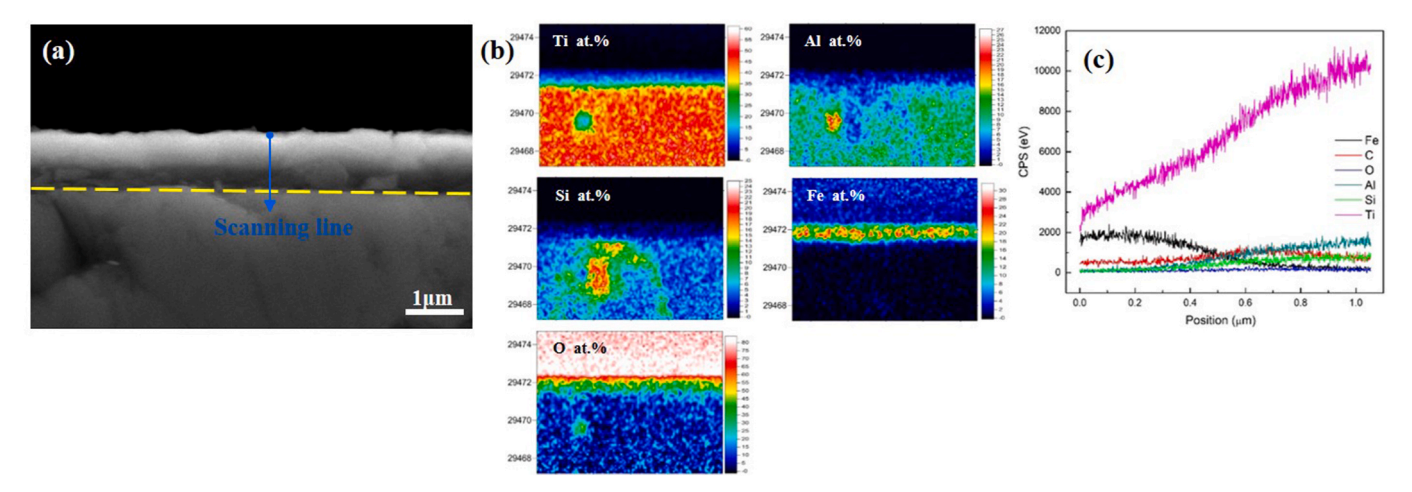


Fig. 7. (a) Cross-sectional SEM image, with (b) elemental WDS map and (c) elemental line analysis along the blue line of the frictional film (a) for  $Ti_3Al_{0.67}Si_{0.28}C_2$  tested at sliding speed of 30 m/s and normal load of 80 N. The arrow line in (a) indicates the scanning direction from outer to inner position. (For interpretation of the references to colour in this figure legend, the reader is referred to the Web version of this article.)

multiphase structure. Fig. 8 shows the XPS spectra of Ti 2p, Al 2p, Sn 3d, Si 2p and Fe 2p detected in the tribo-film formed on  $Ti_3Al_{0.94}C_2$ ,  $Ti_3Al_{0.78}Sn_{0.22}C_2$  and  $Ti_3Al_{0.67}Si_{0.28}C_2$  sliding surfaces after dry sliding under normal load of 80 N with sliding speed of 30 m/s. As to the XPS spectrum of Ti 2p (Fig. 8a), the bonding energies at 458.7 eV and 465.4 eV can be assigned to Ti  $2p_{3/2}$  and Ti  $2p_{1/2}$  in TiO<sub>2</sub> [14,41]. The main Ti 2p peaks for tribo-films formed at  $Ti_3Al_{0.78}Sn_{0.22}C_2$  and  $Ti_3Al_{0.67}Si_{0.28}C_2$  are slightly shifted when compared to that detected in the tribo-film formed on  $Ti_3Al_{0.94}C_2$ , but they can still be associated with Ti in TiO<sub>2</sub>. In the Al 2p XPS spectrum (Fig. 8b), the peaks can be attributed to Al in  $Al_2O_3$  for all three samples [14,41], while peaks in XPS spectra for Fe 2p (Fig. 8c) can be associated with binding energies in Fe<sub>2</sub>O<sub>3</sub> [41]. The binding energy of Sn 3d peaks at 498.95 and 486.05 eV (Fig. 8d) are

associated with  $SnO_2$ , while the binding energies for the Si 2p peaks (Fig. 8e) of 101.95 and 104.1 eV suggests formation of  $Al_2SiO_5$  and  $SiO_2$  in the tribo-film [41]. Obviously, the characteristic XPS peaks of MAX and MAX solid solutions disappeared after sliding, indicating that the tribo-film formed on the sliding surface contains only Ti, Al, Sn and Si oxides.

Last but not least, the sliding debris generated during dry sliding testing of  ${\rm Ti}_3{\rm Al}_{0.94}{\rm C}_2$ ,  ${\rm Ti}_3{\rm Al}_{0.78}{\rm Sn}_{0.22}{\rm C}_2$  and  ${\rm Ti}_3{\rm Al}_{0.67}{\rm Si}_{0.28}{\rm C}_2$  was collected and examined under SEM. Fig. 9a–c shows selected but typical SEM micrographs of the sliding debris, while Fig. 9d–f shows corresponding EDS results for wear debris generated during dry sliding test at 80 N and sliding speed of 30 m/s. As it can be seen in Fig. 9, for most of the wear debris have a flake-like shape, suggesting that it forms because

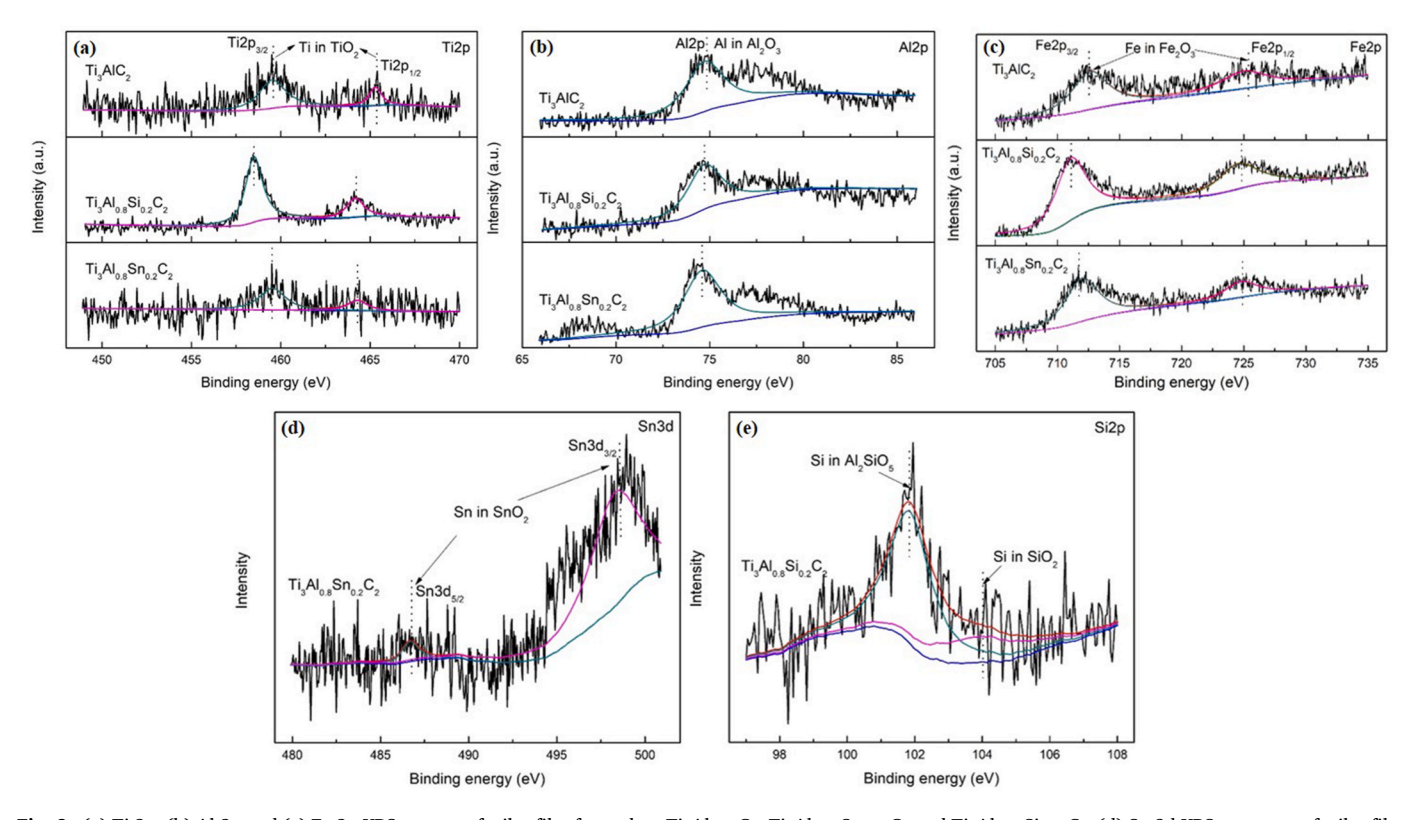


Fig. 8. (a) Ti 2p, (b) Al 2p and (c) Fe 2p XPS spectra of tribo-film formed on  $Ti_3Al_{0.78}C_2$ ,  $Ti_3Al_{0.78}Sn_{0.22}C_2$  and  $Ti_3Al_{0.67}Si_{0.28}C_2$ ; (d) Sn 3d XPS spectrum of tribo-film formed on  $Ti_3Al_{0.78}Sn_{0.22}C_2$ ; (e) Si XPS spectrum of tribo-film formed on  $Ti_3Al_{0.67}Si_{0.28}C_2$  after tribo-testing at sliding rate of 30 m/s under 80 N normal load.

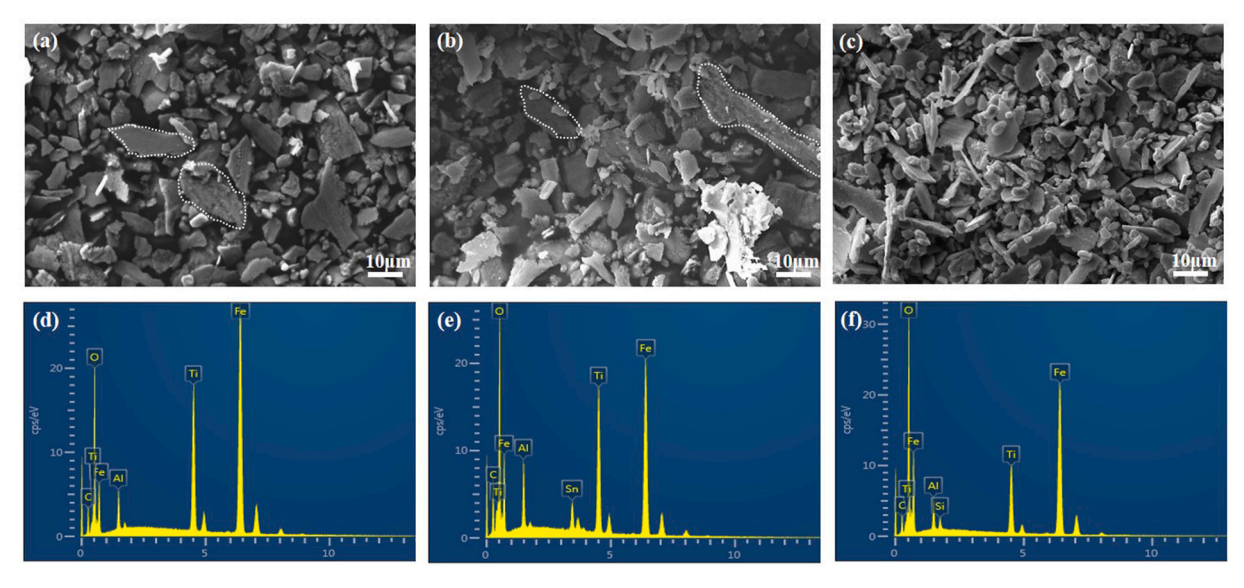


Fig. 9. SEM micrographs of wear debris collected during dry sliding testing of (a)  $Ti_3Al_{0.94}C_2$ , (b)  $Ti_3Al_{0.78}Sn_{0.22}C_2$  and (c)  $Ti_3Al_{0.67}Si_{0.28}C_2$  and corresponding EDS analysis of wear debris collected during dry sliding testing of (d)  $Ti_3Al_{0.94}C_2$ , (e)  $Ti_3Al_{0.78}Sn_{0.22}C_2$  and (f)  $Ti_3Al_{0.67}Si_{0.28}C_2$ .

of the tribo-film peeling (or spallation) during dry sliding test. For Ti<sub>3</sub>Al<sub>0.94</sub>C<sub>2</sub> and Ti<sub>3</sub>Al<sub>0.78</sub>Sn<sub>0.22</sub>C<sub>2</sub>, a few relatively larger tracts of wear debris were observed in SEM (circled by dished lines in Fig. 9a and b), while the wear debris collected during dry sliding of Ti<sub>3</sub>Al<sub>0.67</sub>Si<sub>0.28</sub>C<sub>2</sub> appears to be more uniform in size (Fig. 9c). More importantly, the EDS results of the wear debris in Fig. 8d-f also suggest that it consists of mixed oxides, similar to that detected by EDS, WDS and XPS in the tribofilm. Therefore, it is reasonable to conclude that wear debris is primarily caused by the tribo-oxide film peeling, instead of directly wearing out the MAX phase matrix [13,27,28,35,36,39]. Therefore, the formation of the tribo-oxide film actually prevents the friction surfaces from wear off, contributing to the good wear resistance of all the three samples. In addition, the fact that large tracts of debris could be seen for Ti<sub>3</sub>Al<sub>0.94</sub>C<sub>2</sub>. and Ti<sub>3</sub>Al<sub>0.78</sub>Sn<sub>0.22</sub>C<sub>2</sub> with lower thickness of tribo-films (Figs. 5–7) but higher wear rates (Fig. 2i) measured under normal load of 80 N at sliding speed of 30 m/s, suggests that peeling and pulverization of the scraps from tribo-oxide film results in the higher wear rate. Therefore, the more oxide is consumed in the formation of the wear debris the more oxide films form on the exposed wear surfaces.

### 4. Discussion

Results of this study show that the tribo-oxidation induced film plays a crucial part in tribological performance of  $Ti_3Al_{0.94}C_2$  MAX phases, and two MAX phase solid solutions, namely  $Ti_3Al_{0.78}Sn_{0.22}C_2$  and  $Ti_3Al_{0.67}Si_{0.28}C_2$ , during dry sliding against S45C steel. It is found that the friction coefficient and wear rate (Fig. 2) are related to the self-generated tribo-films during sliding (Fig. 3) on the friction surface, the properties of that film and its adhesion to the matrix MAX phase (Figs. 4–9).

It is precisely because of the tribo-induced oxidation that facilitates the formation of those self-generated friction films on the sliding surface during dry sliding against S45C steel, as it can be concluded form the EDS, WDS and XPS analysis of the tribo-films (Table 2 and Figs. 4–8). EDS analysis (Table 2 and Figs. 4–6) shows very small amount of Fe on the friction surface after sliding test at sliding speeds 30 m/s, this limited transfer of Fe into the tribo-oxide film can be attributed to the fact that smooth and compact tribo-oxide film fully covering the sliding surface forms primarily by the tribo-oxidation of primarily the MAX phase matrices.

When put in the conjunction with previously published results [13, 27,28,35,36,39], this study clearly shows that sliding speed and normal

load as the external variables, have significant effect on tribological film formation in MAX phases. As it can be concluded from results presented in Figs. 2, 3 and 9, the friction surface is ploughed and scratched heavily at lower sliding speed and normal load. It consequently leads to higher friction coefficients and wear rates under those testing conditions. Subsequently, as sliding speed and normal load increase, wear debris were impacted and compacted into continuous and smooth tribo-films adhered to the sliding surface, which is favorable for reducing the friction coefficient. Previous studies [13,27,28,35,36,39] have also demonstrated that the wear debris formed films acted as lubricants in MAX phases, and thus the MAX phases that form compact and stable tribo-film in this study exhibited excellent wear resistance under high sliding speed and normal loads. Indeed, as it can be seen in Fig. 3 for Ti<sub>3</sub>Al<sub>0.94</sub>C<sub>2</sub>, Ti<sub>3</sub>Al<sub>0.78</sub>Sn<sub>0.22</sub>C<sub>2</sub> and Ti<sub>3</sub>Al<sub>0.67</sub>Si<sub>0.28</sub>C<sub>2</sub>, coverage of sliding surface with compact and stable tribo-films increases with increasing sliding speed from 10 to 30 m/s resulting in obvious decrease in friction coefficients in Fig. 2. Therefore, it is reasonable to conclude that the wear mechanisms can be attributed to abrasion wear caused by debris particles and adhesive wear at lower sliding speeds and normal load, while it changes to the two body abrasion wear and oxidation wear as sliding speed and normal load increase.

In general, the higher sliding speed accelerates the generation of oxides due to the higher tribo-induced instantaneous temperature, such a tribo-oxidation process depends on the frictional heat, that is proportional to the normal load, sliding speed, as well as the friction coefficient. Actually, the tribo-oxidation is identified as a dynamic oxidation process of oxide formation, its consumption due to peeling of the surface and re-oxidation of oxide-free surfaces [13,27,28]. With the continuous formation of the tribo-oxide film, the oxides would be consumed as wear debris form during sliding. Subsequently, once the tribo-films happens to peel off, new ones could be formed by tribo-oxidation. In order to generate and maintain the tribo-oxide film on the friction surface, it is necessary to satisfy that the generating rate is larger than the consuming rate [42]. Therefore, the redundant oxides will be peeled off as wear debris, resulting into larger wear rate by degrees for Ti<sub>3</sub>Al<sub>0.94</sub>C<sub>2</sub> and Ti<sub>3</sub>Al<sub>0.78</sub>Sn<sub>0.22</sub>C<sub>2</sub> when comparted to Ti<sub>3</sub>Al<sub>0.67</sub>Si<sub>0.28</sub>C<sub>2</sub> in this work. Herein, the result shows that at sliding speeds of 10 and 20 m/s, wear rates of Ti<sub>3</sub>Al<sub>0.67</sub>Si<sub>0.28</sub>C<sub>2</sub> were larger than those of Ti<sub>3</sub>Al<sub>0.94</sub>C<sub>2</sub>, but lower at sliding rates of 30 m/s.

Results of this study also show that the chemical phase constitution and physical states of the formed tribo-film were responsible for the tribological behaviors of MAX phases [36], since  $Ti_3Al_{0.94}C_2$ ,

Ti<sub>3</sub>Al<sub>0.78</sub>Sn<sub>0.22</sub>C<sub>2</sub> and Ti<sub>3</sub>Al<sub>0.67</sub>Si<sub>0.28</sub>C<sub>2</sub> exhibited different tribological performance. Partially substituting Al with Sn or Si to form Ti<sub>3</sub>Al<sub>0.78</sub>Sn<sub>0.22</sub>C<sub>2</sub> and Ti<sub>3</sub>Al<sub>0.67</sub>Si<sub>0.28</sub>C<sub>2</sub> affected the combination of mixed oxides with formation of an extra tin oxides and silicon oxides. As for Ti<sub>3</sub>Al<sub>0.67</sub>Si<sub>0.28</sub>C<sub>2</sub>, the formation of aluminosilicate glassy phases of Al<sub>2</sub>SiO<sub>5</sub> and SiO<sub>2</sub> in tribo-oxide film has been detected using XPS. The glassy phases played an important role in the friction and wear performance of Ti<sub>3</sub>Al<sub>0.75</sub>Si<sub>0.25</sub>C<sub>2</sub>, since they are glassy and even maybe in the liquid form at high temperatures during sliding and thus they can easily fill pores and micro-cracks during the sliding, which might increase the bonding strength of tribo-layers [43,44]. In addition to this, liquid state oxides were hardly to peeled off as wear debris. Accordingly, wear rates of Ti<sub>3</sub>Al<sub>0.75</sub>Si<sub>0.25</sub>C<sub>2</sub> decreased with the sliding speed increase from 20 to 80 N. Formation of tin oxide on sliding surfaces has been shown to adjust the friction coefficient of Ti<sub>3</sub>Al(Sn)C<sub>2</sub> within the range of 0.13-0.33 [36]. Previous study [45] showed that the substitution of Al by Sn led to a non-protective SnO2 layer that forms first during the oxidation of Ti<sub>3</sub>Al<sub>0.8</sub>Sn<sub>0.2</sub>C<sub>2</sub> at 800-1000 °C and lead to the formation of a multilayered tribo-film consisting of TiO2, SnO2, and Al2O3. The presence of Sn in the solid solution promoted the oxidation process. Given this, when Ti<sub>3</sub>Al<sub>0.78</sub>Sn<sub>0.22</sub>C<sub>2</sub> was tested in dry sliding at high speeds and normal loads in this work, the more tribo-oxide layers formed and they peeled off easier as large tracts of debris (see Fig. 9), resulting into higher wear rate.

On the basis of the above discussion, it is practicable to adjust the tribological performance of  ${\rm Ti}_3{\rm Al}_{0.94}{\rm C}_2$  phase to enlarge its application by adding various A-site elements to prepare A-site solid solutions.

#### 5. Conclusions

In this work, dry sliding behaviors of hot pressed  $\rm Ti_3Al_{0.94}C_2$ ,  $\rm Ti_3Al_{0.78}Sn_{0.22}C_2$  and  $\rm Ti_3Al_{0.67}Si_{0.28}C_2$  samples against S45C steel counterpart disk in the normal load range of 20–80 N and sliding speed range of 10–30 m/s were investigated. The results of the study show that:

- (1) The friction coefficient and wear rate were strongly influenced by sliding speed and normal load for all three MAX phases.
- (2) The wear mechanisms were combination of abrasion wear caused by debris particles and adhesive wear at lower sliding speeds and normal load, while it changed to the two body abrasion wear and oxidation wear with increasing the sliding speed and normal load.
- (3) The friction coefficient of  $Ti_3Al_{0.67}Si_{0.28}C_2$  was found to be higher than that of  $Ti_3Al_{0.94}C_2$ , while friction coefficient of  $Ti_3Al_{0.94}C_2$  was found to be higher than that of  $Ti_3Al_{0.78}Sn_{0.22}C_2$ . It could be adapted within the friction coefficient range of 0.2–0.38 after partial substitution of Al by Sn and Si in  $Ti_3Al_{0.94}C_2$  while retaining excellent wear resistance. Thus, substitution of Al with Sn and Si can be used to adjust friction coefficients of  $Ti_3Al_{0.94}C_2$  to that needed for the particular application.
- (4) The chemical phase composition and physical states of the dominated tribo-oxide film were responsible for observed tribological behavior. The tribo-films contained of a Fe-rich oxide on the outer surface, while inner layers of the tribo-film contained Ti and Al oxides, and in the cases of Ti<sub>3</sub>Al<sub>0.78</sub>Sn<sub>0.22</sub>C<sub>2</sub> and Ti<sub>3</sub>Al<sub>0.67</sub>Si<sub>0.28</sub>C<sub>2</sub>. Sn and Si oxides, respectively.

# Declaration of competing interest

The authors declare that they have no known competing financial interests or personal relationships that could have appeared to influence the work reported in this paper.

#### Acknowledgment

This work was supported by the Fundamental Research Funds for the Central Universities under Grant No. 2018YJS146, by National Science Foundation of China (NSFC) under Grant Nos. 51572017 and 51871011, by the program of China Scholarships Council (CSC) under Grant CSC No. 201807090027, and by United States National Science Foundation (NSF) under the grant No. 1729350. The financial support from funding agencies is greatly appreciated. We also thank Dr. Andrew Mott (Texas A&M University) for help with EPMA analysis.

#### References

- W.C. Wang, Application of a high temperature self-lubricating composite coating on steam turbine components, Surf. Coating. Technol. 177–178 (2004) 12–17.
- [2] C. Muratore, A.A. Voevodin, Chameleon coatings: adaptive surfaces to reduce friction and wear in extreme environments, Annu. Rev. Mater. Res. 39 (2009) 297–324.
- [3] S.M. Aouadi, B. Luster, P. Kohli, C. Muratore, A.A. Voevodin, Progress in the development of adaptive nitride-based coatings for high temperature tribological applications, Surf. Coating. Technol. 204 (2009) 962–968.
- [4] M.W. Barsoum, The  $M_{N+1}AX_N$  phases: a new class of solids: thermodynamically stable nanolaminates, Prog. Solid State Chem. 28 (2000) 201–281.
- [5] Z.M. Sun, Progress in research and development on MAX phases: a family of layered ternary compounds, Int. Mater. Rev. 56 (2011) 143–166.
- [6] M. Radovic, M.W. Barsoum, MAX phases: bridging the gap between metals and ceramics, Am. Ceram. Soc. Bull. 92 (2013) 20–27.
- [7] Y.W. Bao, X.H. Wang, H.B. Zhang, Y.C. Zhou, Thermal shock behavior of Ti<sub>3</sub>AlC<sub>2</sub> from between 200 °C and 1300 °C, J. Eur. Ceram. Soc. 25 (2005) 3367–3374.
- [8] M.W. Barsoum, M. Radovic, Elastic and mechanical properties of the MAX phases, Annu. Rev. Mater. Res. 41 (2011) 195–227.
- [9] D.J. Tallman, B. Anasori, M.W. Barsoum, A critical review of the oxidation of Ti<sub>2</sub>AlC, Ti<sub>3</sub>AlC<sub>2</sub> and Cr<sub>2</sub>AlC in air, Mater. Res. Lett. 1 (2013) 115–125.
- [10] S.B. Li, G.M. Song, K. Kwakernaak, S.V.D. Zwaag, W.G. Sloof, Multiple crack healing of a Ti<sub>2</sub>AlC ceramic, J. Eur. Ceram. Soc. 32 (2012) 1813–1820.
- [11] N.V. Tzenov, M.W. Barsoum, Synthesis and characterization of Ti<sub>3</sub>AlC<sub>2</sub>, J. Am. Ceram. Soc. 83 (2000) 825–832.
- [12] Y. Zhang, G.P. Ding, Y.C. Zhou, Ti<sub>3</sub>SiC<sub>2</sub>-a self-lubricating ceramic, Mater. Lett. 55
- [13] H.X. Zhai, Z.Y. Huang, M.X. Ai, Z. Yang, Z.L. Zhang, S.B. Li, Tribophysical properties of polycrystalline bulk Ti<sub>3</sub>AlC<sub>2</sub>, J. Am. Ceram. Soc. 88 (2005) 3270, 3274
- [14] J.Q. Ma, J.Y. Hao, L.C. Fu, Z.H. Qiao, J. Yang, W.M. Liu, et al., Intrinsic self-lubricity of layered Ti<sub>3</sub>AlC<sub>2</sub> under certain vacuum environment, Wear 297 (2013)
- [15] S. Gupta, M.W. Barsoum, On the tribology of the MAX phases and their composites during dry sliding: a review, Wear 271 (2011) 1878–1894.
- [16] J.Q. Ma, F. Li, J. Cheng, L.C. Fu, Z.H. Qiao, W.M. Liu, et al., Tribological behavior of Ti<sub>3</sub>AlC<sub>2</sub> against SiC at ambient and elevated temperatures, Tribol. Lett. 50 (2013) 323–330.
- [17] S. Wang, J.Q. Ma, S.Y. Zhu, J. Cheng, Z.H. Qiao, J. Yang, et al., High temperature tribological properties of Ti<sub>3</sub>AlC<sub>2</sub> ceramic against SiC under different atmospheres, Mater. Des. 67 (2015) 188–196.
- [18] P. Kar, S. Kundu, M. Radovic, L.F. Hu, Tribofilm formation using Ti<sub>2</sub>AlC material, in: K. Lu, N. Manjooran, M. Radovic, E. Medvedovski, E.A. Olevsky, C. Li, G. Singh, N. Chopra, G. Pickrell (Eds.), Advances in Nanomaterials and Nanostructures, John Wiley & Sons Inc., Hoboken, 2011, pp. 187–193.
- [19] G.M. Song, Y.T. Pei, W.G. Sloof, S.B. Li, J.T.M. De Hosson, S. van der Zwaag, Oxidation-induced crack healing in Ti<sub>3</sub>AlC<sub>2</sub> ceramics, Scripta Mater. 58 (2008) 13-16
- [20] S. Basu, N. Obando, A. Gowdy, I. Karaman, M. Radovic, Long-term oxidation of Ti<sub>2</sub>AlC in air and water vapor at 1000-1300°C temperature range, J. Electrochem. Soc. 159 (2012) C90–C96.
- [21] J.W. Byeon, J. Liu, M. Hopkins, W. Fischer, N. Garimella, K.B. Park, et al., Microstructure and residual stress of alumina scale formed on Ti<sub>2</sub>AlC at high temperature in air, Oxid. Metals 68 (2008) 97–111.
- [22] H.J. Yang, Y.T. Pei, J.C. Rao, J.M. Th, D. Hosson, Self-healing performance of Ti-AlC ceramic, J. Mater. Chem. 22 (2012) 8304–8313.
- [23] Z.Y. Huang, J. Bonneville, H.X. Zhai, V. Gauthier-Brunet, S. Dubois, Microstructural characterization and compression properties of TiC<sub>0.61</sub>/Cu(Al) composite synthesized from Cu and Ti<sub>2</sub>AlC<sub>2</sub> powders, J. Alloys Compd. 602 (2014) 53–57.
- [24] W.J. Wang, H.X. Zhai, L.L. Chen, Z.Y. Huang, G.P. Bei, P. Greil, Preparation and mechanical properties of TiC<sub>x</sub>-(NiCu)<sub>3</sub>Al-CuNi<sub>2</sub>Ti-Ni hybrid composites by reactive pressureless sintering pre-alloyed Cu/Ti<sub>3</sub>AlC<sub>2</sub> and Ni as precursor, Mater. Sci. Eng. 670 (2016) 351–356.
- [25] L.F. Hu, A. Kothalkar, G. Proust, I. Karaman, M. Radovic, Fabrication and characterization of NiTi/Ti<sub>2</sub>SiC<sub>2</sub> and NiTi/Ti<sub>2</sub>AlC composites, J. Alloys Compd. 610 (2014) 635–644.
- [26] W.Q. Hu, Z.Y. Huang, L.P. Cai, C. Lei, H.X. Zhai, S.M. Hao, et al., Preparation and mechanical properties of TiC<sub>X</sub>-Ni<sub>3</sub>(Al,Ti)/Ni composites synthesized from Ni alloy and Ti<sub>3</sub>AlC<sub>2</sub> powders, Mater. Sci. Eng. 697 (2017) 48–54.

- [27] H.X. Zhai, Z.Y. Huang, Y. Zhou, Z.L. Zhang, Y.F. Wang, M.X. Ai, Oxidation layer in sliding friction surface of high-purity Ti<sub>3</sub>SiC<sub>2</sub>, J. Mater. Sci. 39 (2004) 6635–6637.
- [28] Z.Y. Huang, H.X. Zhai, M.L. Guan, X. Liu, M.X. Ai, Y. Zhou, Oxide-film-dependent tribological behaviors of Ti<sub>3</sub>SiC<sub>2</sub>, Wear 262 (2007) 1079–1085.
- [29] Z.Y. Huang, H.X. Zhai, Y. Zhou, Y.F. Wang, Z.L. Zhang, Sliding friction behavior of bulk Ti<sub>3</sub>SiC<sub>2</sub> under different normal pressures, Key Eng. Mater. 280/283 (2005) 1353–1356.
- [30] G.P. Bei, V. Gauthier-Brunet, C. Tromas, S. Dubois, Synthesis, characterization, and intrinsic hardness of layered nanolaminate Ti<sub>3</sub>AlC<sub>2</sub> and Ti<sub>3</sub>Al<sub>0.8</sub>Sn<sub>0.2</sub>C<sub>2</sub> solid solution, J. Am. Ceram. Soc. 95 (2012) 102–107.
- [31] S. Dubois, G.P. Bei, C. Tromas, V. Gauthier-Brunet, P. Gadaud, Synthesis, microstructure, and mechanical properties of Ti<sub>3</sub>Sn<sub>(1-x)</sub>Al<sub>x</sub>C<sub>2</sub> MAX phase solid solutions, Int. J. Appl. Ceram. Technol. 7 (2010) 719–729.
- [32] Y.C. Zhou, J.X. Chen, J.Y. Wang, Strengthening of Ti<sub>3</sub>AlC<sub>2</sub> by incorporation of Si to form Ti<sub>3</sub>Al<sub>1-x</sub>Si<sub>x</sub>C<sub>2</sub> solid solutions, Acta Mater. 54 (2006) 1317–1322.
- [33] L.P. Cai, Z.Y. Huang, W.Q. Hu, C. Lei, S.S. Wo, X.K. Li, et al., Fabrication and microstructure of a new ternary solid solution of Ti<sub>3</sub>Al<sub>0.8</sub>Si<sub>0.2</sub>Sn<sub>0.2</sub>C<sub>2</sub> with high solid solution strengthening effect, Ceram. Int. 44 (2018) 9593–9600.
- [34] H.L. Gao, R. Benitez, W. Son, R. Arroyave, M. Radovic, Structural, physical and mechanical properties of Ti<sub>3</sub>(Alx<sub>1-x</sub>Si<sub>x</sub>)C<sub>2</sub> solid solution with x=0-1, Mater. Sci. Eng. 676 (2016) 197–208.
- [35] H. Xu, Z.Y. Huang, H.X. Zhai, M.Q. Li, X.H. Liu, Y. Zhou, Fabrication, mechanical properties, and tribological behaviors of Ti<sub>3</sub>Al<sub>0.8</sub>Sn<sub>0.4</sub>C<sub>2</sub>Solid solution by two-time hot-pressing method, Int. J. Appl. Ceram. Technol. 12 (2015) 783–789.
- [36] Z.Y. Huang, H. Xu, H.X. Zhai, Y.Z. Wang, Y. Zhou, Strengthening and tribological surface self-adaptability of Ti<sub>3</sub>AlC<sub>2</sub> by incorporation of Sn to form Ti<sub>3</sub>Al(Sn)C<sub>2</sub> solid solutions, Ceram. Int. 41 (2015) 3701–3709.

- [37] S.B. Li, G.P. Bei, C.W. Li, M.X. Ai, H.X. Zhai, Y. Zhou, Synthesis and deformation microstructure of Ti<sub>3</sub>SiAl<sub>0.2</sub>C<sub>1.8</sub> solid solution, Mater. Sci. Eng. 441 (2006) 202-205
- [38] A. Ganguly, T. Zhen, M.W. Barsoum, Synthesis and mechanical properties of Ti<sub>3</sub>GeC<sub>2</sub> and Ti<sub>3</sub>(Si<sub>x</sub>Ge<sub>1-x</sub>)C<sub>2</sub> (x=0.5, 0.75) solid solutions, J. Alloys Compd. 376 (2004) 287–295.
- [39] L.P. Cai, Z.Y. Huang, W.Q. Hu, C. Lei, H.X. Zhai, Y. Zhou, Dry sliding behaviors and friction surface characterization of Ti<sub>3</sub>Al<sub>0.8</sub>Si<sub>0.2</sub>Sn<sub>0.2</sub>C<sub>2</sub> solid solution against S45C steel, Ceram. Int. 45 (2018) 2103–2110.
- [40] H.X. Zhai, Z.Y. Huang, Instabilities of sliding friction governed by asperity interference mechanisms, Wear 257 (2004) 414–422.
- [41] J.F. Moulder, W.F. Stickle, P.E. Sobol, K.D. Bomben, Handbook of X-Ray Photoelectron Spectroscopy, Physical Electronics Inc., Eden Prairie, Minnesota, 1992, pp. 55–127.
- [42] J.R. Barber, Thermoelastic instabilities in the sliding of comforming solids, Proc. R. Soc. A. 312 (1969) 381–394.
- [43] J.X. Chen, Y.C. Zhou, Effect of Si content on the oxidation resistance of  $Ti_3Al_1$ .  ${}_xSi_xC_2$  (x $\leq$ 0.25) solid solutions at 1000–1400°C in air, Oxid. Metals 65 (2006) 123–135
- [44] S. Li, G.M. Song, Y. Zhou, A dense and fine-grained SiC/Ti<sub>2</sub>Si(Al)C<sub>2</sub> composite and its high-temperature oxidation behavior, J. Eur. Ceram. Soc. 32 (2012) 3435–3444.
- [45] E. Drouelle, V. Brunet, J. Cormier, P. Villechaise, S. Dubois, Oxidation resistance of Ti<sub>3</sub>AlC<sub>2</sub> and Ti<sub>3</sub>AlO<sub>8</sub>Sn<sub>0.2</sub>C<sub>2</sub> MAX phases: a comparison, J. Am. Ceram. Soc. 103 (2019) 1270–1280.